Monte Carlo Study of the Stabilization of Complex Bicontinuous Phases in Diblock Copolymer Systems

Francisco J. Martínez-Veracoechea and Fernando A. Escobedo*

School of Chemical and Biomolecular Engineering, Cornell University, Ithaca, New York 14853

Received June 29, 2007; Revised Manuscript Received July 28, 2007

ABSTRACT: Lattice Monte Carlo simulations are used to study the stabilization of different ordered bicontinuous phases in A−B diblock copolymer systems. The stabilization approach involves attempting to reduce the packing frustration inside the nodes of the bicontinuous phases by the addition of an A-component "additive". Two different strategies are considered which entail the addition of (1) explicit selective-solvent particles and (2) homopolymer of a length equal to 80% that of the diblock copolymer chains. Approximate phase boundaries were found via free-energy calculations, and great care was taken to enact the commensurability of system size with the unit-cell dimensions of distinct candidate phases. A very contrasting phase behavior is observed upon increasing the amount of the A-component additive in the two different strategies. With the first strategy (i.e., addition of solvent particles) we observed the progression gyroid → perforated lamella → lamella → reversed gyroid, including a long-lived metastable orthorhombic cocontinuous phase known as O^{52}. With the second strategy (i.e., addition of homopolymer) we observed the progression of morphologies gyroid → double diamond → plumber's nightmare. In the latter two bicontinuous phases, the homopolymer concentrates preferentially in the nodes not only to reduce the nodal packing frustration but also to enhance the homopolymer's conformational entropy. At high homopolymer volume fractions, a novel morphology was observed, wherein cylinders of two different diameters alternate in a tetragonal (square) packing; however, it remains unclear whether this "alternating diameter cylinder" phase is just a long-lived metastable or a truly stable phase at some of the conditions examined. The dissimilarity in the resulting phase behavior for the two strategies considered is rationalized in terms of the difference in the degree of penetration of the two additives into the diblock copolymer layer, which is a direct consequence of the disparity in translational entropy exhibited by the homopolymers and by the solvent particles.

I. Introduction

The capacity of block copolymer systems to self-assemble at mesoscopic length scales has made them the focus of extensive research.[1,2] Particular attention has been paid to pure diblock copolymer (DBC) melts where different morphologies of specific geometry can be rationally obtained just by adjusting the relative sizes of the two blocks.[1,3] By this means, a number of distinct mesophases can be obtained: spheres with bcc packing (S), cylinders hexagonally packed (C), the lamellar phase (L), the bicontinuous gyroid phase[3,4] (G), and the recently observed cocontinuous O^{70} phase.[5,6] A perforated lamellae phase (PL) is often observed in experiments[7] and simulations;[8,9] however, this phase has been proven to be just a long-lived metastable state in the bulk of the pure DBC melt phase diagram.[10,11]

Of great scientific and technological interest is a particular kind of mesophase based in minimal surfaces, known as the ordered bicontinuous phases.[12] In these phases the minority component forms two triply periodic interweaving networks that never intersect, making them ideal candidates as precursor of: porous materials,[13,14] regular three-dimensional networks, and high-conductivity nanocomposites.[15] Experimentally, some systems of surfactants have been observed to present a rich variety of these phases. For example, Ström and Anderson[16] observed in the system didodecyldimethylammonium bromide−water−styrene a progression of the bicontinuous phases gyroid (G), double diamond (DD), plumber's nightmare (P), and Neovius' surface [*C*(*P*)]. However, pure DBC melts present a much more limited variety of bicontinuous phases. While in pure DBC melts it was initially thought that the stable bicontinuous phase was the DD phase, it is now well-established that the only stable bicontinuous phase in pure DBC melts is the G phase.[4,17,18]

A common feature of the ordered bicontinuous phases is that their minority-component networks form a structure composed of tubes (connectors) and nodes.[19] The number of tubes intersecting in each node depends upon the specific phase. For example, the numbers of tubes that intersect in the nodes of the G, DD, and P phases are three, four, and six tubes, respectively. While the thickness of the tubes is roughly determined by the minority-component block length, the thickness of the nodes (which are formed by the junction of several tubes) is necessarily bulkier in order to approach the constant-mean-curvature (cmc) structure that will minimize the interfacial energy.[19] As a result, the DBC chains cannot reach the center of the nodes without either stretching or deforming the node's shape, causing an entropically unfavorable scenario known as packing frustration. It has been suggested[3,19] that the reason for the limited stability of the bicontinuous phases in the pure DBC melt is the existence of packing frustration inside the nodes. Moreover, it has also been argued[19] that since the G phase is the bicontinuous phase with the smallest number of tubes per node, and therefore with the smallest nodes, the G phase is the ordered bicontinuous phase with the least packing frustration, and hence, the only stable one in pure DBC melts.

In previous works,[20,21] we were able to detect direct evidence of packing frustration inside the G phase nodes. Additionally, we used bidispersity as a means to alleviate the frustration, achieving the stabilization of the G phase in a wider range of temperatures.[20] The frustration in the nodes could also be alleviated by the addition of small quantities of other "fillers" or "additives" like selective nanoparticles or homopolymer (Figure 1) that would preferentially concentrate inside the

* Corresponding author. E-mail: fe13@cornell.edu.

10.1021/ma071449g CCC: $37.00
Published on Web 09/08/2007

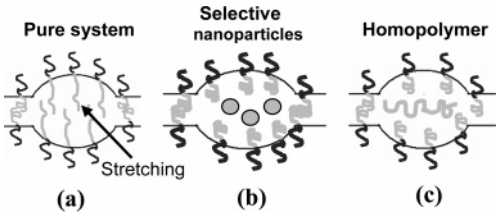

Figure 1. Cartoon representing (a) how packing frustration can manifest in the form of chain stretching in the nodes of the bicontinuous phases of pure DBC systems and two strategies that can be used to alleviate this nodal frustration: (b) via selective nanoparticles and (c) via homopolymers.

nodes.[22] In principle, this reduced frustration can be used not only to increase the range of stability of the G phase but also to stabilize other bicontinuous phases like the DD and P.[19] Indeed, in systems of triblock copolymers, Dotera[23] performed lattice Monte Carlo (MC) simulations where a progression of the form "single" G → "single" D → and "single" P was observed by the addition of homopolymer. In DBC systems, however, the situation is less clear. On one hand, mean-field SCFT has been used to predict the stabilization of the DD phase in a very narrow region of the phase diagram by the addition of homopolymer.[24] On the other hand, the Wiesner Group[25,26] has realized a series of experiments in a mixture of a diblock copolymer (e.g., PI-*b*-PEO) with an inorganic aluminosilicate, for which the P phase was observed but the DD was not.

Although SCFT has proven to be a very useful tool in resolving many of the issues regarding the phase behavior of block copolymer systems,[27−29] in the present work we will adopt the more straightforward (though more time-consuming) particle-based approach, wherein the effects of finite chain length size and local density fluctuations are naturally incorporated. Particle-based simulations have been relatively successful in showing the stabilization of the G and PL phases in DBC systems with a selective solvent.[30−35] However, to the best of our knowledge, a particle-based approach has never been used to predict the stabilization of ordered bicontinuous phases, different from the G phase, in DBC melt systems. Moreover, even though extensive work has been done in the area of block copolymer/nanoparticle composites,[2,36,37] these results did not treat the bicontinuous phases and concentrated in the "classical" (i.e., the L, C, and S phases) morphologies.

In the present paper, we perform lattice MC simulations to study the stabilization of different complex phases through the reduction of packing frustration. Two different strategies are considered which aim to counter the frustration effects by addition of minority (A) component in the form of (1) selective solvent particles of size comparable to the polymer Kuhn length (i.e., monomeric solvent) and (2) homopolymer of a chain length equal to 80% that of the copolymer chains. In order to be able to observe the bicontinuous phases, simulations were carried out at conditions where the G phase has previously been observed for the pure melt in lattice systems (i.e., $\chi N = 40$ and volume fraction of A-block = 0.30).[20] A surprisingly different phase behavior is observed upon increasing the amount of the A-component additive in the two different cases. With the first strategy (i.e., addition of solvent particles) we observed the progression G → PL → L→ reversed gyroid (RG), with the PL phase sharing the phase diagram with a long-lived metastable orthorhombic cocontinuous network phase known as O[52]. With the second strategy (i.e., addition of homopolymer) we observed the mesophase progression G → DD → P. In both, the DD and the P phases, the homopolymer was observed to preferentially concentrate in the nodes, consistent with the idea of reduction of the packing frustration. Additionally, in regions with homopolymer concentration equal to or greater than the concentration where the P phase was found, a novel morphology was observed, wherein cylinders of two different diameters alternate in a tetragonal (square) packing. The difference observed in the phase behavior for the two strategies considered is rationalized in terms of the difference in translational (mixing) entropy between the solvent particles and the homopolymer.

II. Model and Methods

A simple cubic lattice is used to discretize space where each site can be occupied only by a single bead of the polymer chain. Each bead in the chain represents a Kuhn segment. Bonds are allowed between the edges of each site as well as between diagonals sites, yielding to a total of 26 neighbors per lattice site. This type of lattice have successfully been used in numerous studies of the phase behavior of surfactant/copolymer systems.[20,30,38]

In this scheme each bead interacts only with its 26 nearest neighbors. The contact energy ϵ_{ij} is defined as

$$\epsilon_{ij} = \begin{cases} 1 & \text{if } i \neq j \\ 0 & \text{if } i = j \end{cases} \tag{1}$$

where i and j represent the type of bead. In DBC systems only two different types of beads are needed: "A" beads (i.e., minority component) and "B" beads (i.e., majority component). The void volume fraction is set to $\eta = 0.25$ to facilitate equilibration.[20]

As is customary for DBC lattice simulations, the Flory−Huggins interaction parameter (χ) is obtained from χ = (number of nonbonded neighbors) × (fraction occupied) × ϵ_{AB}/kT

$$\chi = 18\beta \tag{2}$$

where $\beta = \epsilon_{AB}/kT$, k is Boltzmann constant, and T is temperature.[23] The DBC composition is defined by

$$f = \frac{\text{number of A beads in chain}}{N} \tag{3}$$

where N is the DBC chain length. Since all beads occupy the same volume, f also defines the volume fraction of A beads in a DBC chain.

In the present work the DBC chain length is set to $N = 20$ with a minority component volume fraction of $f = 0.30$. Such a chain length has been successfully used by several authors[20,21,23,39] to study the phase behavior of DBC systems, indicating that it provides a good compromise between computational efficiency and suitable representation of the DBC. Additionally, the simulation conditions will be fixed at $\beta = 0.1111$ (i.e., $\chi N = 40$) since it has been found that at these conditions the pure DBC melt for this model presents a stable gyroid phase.[20]

The selective solvent particles are explicitly represented by a single A bead (i.e., each solvent particle occupies only a single lattice site). The homopolymer is represented as chains of A beads, with a chain length of $N_{ho} = 16$. The fraction of nonempty sites occupied by the "additive" (i.e., either solvent or homopolymer) is denoted by ϕ_{add}.

Simulations are carried out according to the *NVT* ensemble Monte Carlo scheme where a set of moves (hops, reptations, and switches)[20] is attempted and accepted with probability given by the standard Metropolis criterion.[40] More details about this

model can be found elsewhere.[20] The "hop", "reptation", and "switching" moves were performed with a relative frequency of 300:30:1, respectively. The systems were equilibrated in the athermal limit and then quenched to the target temperature (i.e., $\beta = 0.1111$) where the systems were left to spontaneously evolve toward a morphology. Simulations were usually run for 8×10^6 MC cycles, of which 2×10^6 MC cycles were for equilibration and the rest for production (when statistics are collected). Each cycle comprised of N_{mon} MC moves where N_{mon} is the total number of monomers in the system.

III. Chemical Potential Calculations

At a given set of thermodynamic conditions, more than one morphology can often spontaneously form depending upon the simulation box size and initial conditions.[20,21,23] The reason is that block copolymer morphologies present long-range ordering, making some structures particularly sensitive to finite-size effects. As a consequence, metastable structures can be stabilized when the simulation box is not of a size commensurate with the unit cell of the stable phase. In the *NVT* ensemble, the most stable phase is the one with the lowest excess Helmholtz free energy per unit chain. Neglecting the PV contributions, which are assumed to be similar and small in different phases with the same density, the stability between phases can be discerned through the excess chemical potential ($\beta\mu^{\mathrm{ex}}$), where the "excess" properties are defined by taking as reference the ideal chain (i.e., a chain having only bonded interactions). In a previous paper[21] we gave a detailed explanation of how to accurately calculate $\beta\mu^{\mathrm{ex}}$ using a variant of the expanded-ensemble (EXE) method.[41,42] In this approach one gradually inserts/removes a target chain in the system by appending/deleting beads to/from it. This method requires a means for accurate estimation of the free energy differences associated with such growth/reduction transitions and the use of suitable biasing weights to attain efficient sampling of all transitions; we adopt here Bennett's acceptance-ratio method[43] to estimate free energy differences and the method of Trebst et al.[44] to get the biasing weights. The partition function of the expanded-ensemble (Q_{EXE}) is defined as

$$Q_{\mathrm{EXE}} = \sum_{m=1}^{M} \exp(\psi_{\mathrm{m}})\, Q(\lambda_{\mathrm{m}}) \tag{4}$$

where $Q(\lambda_m)$ in our case is the partition function of the *NVT* ensemble with characteristic parameter λ_m (e.g., the number of target-chain beads already inserted), and ψ_m is an arbitrary bias weighting function that is optimized to obtain efficient sampling[21] by means of a modification of the method of Trebst et al.[44]

If the insertion/deletion attempts are proposed with equal probability, the Metropolis acceptance criterion for a macrostate transition $m \rightarrow m + \Delta$, with configurational-bias sampling, biased only according to excluded volume interactions, becomes

$$P_{\mathrm{acc}} = \min\{1, \exp(-\upsilon + \psi_{m+\Delta} - \psi_m)\} \tag{5}$$

with

$$\upsilon = -\Delta \ln W + \beta(U_{m+\Delta} - U_m) \tag{6}$$

where $\Delta = +1$ for growth, $\Delta = -1$ for reduction, U is the interaction energy, and W is the Rosenbluth weight[40] calculated with excluded volume interactions alone for the corresponding insertion/deletion process. Macrostate transitions were attempted with a frequency of two attempts per MC cycle.

The Helmholtz free energy (A) differences associated with the insertion/deletion of a bead in the target chain can be estimated using Bennett's acceptance ratio formula:

$$\beta A(\lambda_{m+1}) - \beta A(\lambda_m) \equiv \ln\left(\frac{Q(\lambda_m)}{Q(\lambda_{m+1})}\right) = C - \ln\left(\frac{\ell_{m+1,m}}{\ell_{m,m+1}}\right) \tag{7}$$

where $\ell_{m,m+1}$ is the number of trial transitions $\lambda_m \rightarrow \lambda_{m+1}$ and C is found from

$$\sum_{m}(1 + \exp[\upsilon(\lambda_m \rightarrow \lambda_{m+1}) - C])^{-1} = \sum_{m+1}(1 + \exp[\upsilon(\lambda_{m+1} \rightarrow \lambda_m) + C])^{-1} \tag{8}$$

where the summation in the left runs over all the $\lambda_m \rightarrow \lambda_{m+1}$ attempted transitions and the summation in the right over all the $\lambda_{m+1} \rightarrow \lambda_m$ attempted transitions. Finally, the excess chemical potential for a single species is calculated from

$$\beta\mu_i^{\mathrm{ex}}(\lambda_1 \rightarrow \lambda_M) = [\beta A(\lambda_M) - \beta A(\lambda_1)] = \sum_{m=1}^{M-1} [\beta A(\lambda_{m+1}) - \beta A(\lambda_m)] \tag{9}$$

Stability between phases is then discerned by comparison of the molar Gibbs free energy of the mixture, βg, calculated as

$$\beta g = \sum y_i\, \beta\mu_i^{\mathrm{ex}} \tag{10}$$

with y_i the mole fraction of species i in the system.

IV. Results and Discussion

Addition of Selective Solvent Particles. The phase behavior of DBC/solvent−particle mixtures was explored for a range of solvent concentrations between $\phi_{\mathrm{add}} = 0.0$ and $\phi_{\mathrm{add}} = 0.40$. A variety of morphologies was observed by changing ϕ_{add}. Among the phases that had been previously reported in DBC systems we observed: the bicontinuous G phase, the PL phase, and the L phase (Figure 2). In addition, an orthorhombic cocontinuous network phase known as O^{52} was also observed (Figure 3). In this phase, the minority component forms a *single* continuous network. The O^{52} phase has never been observed in DBC systems and has only been reported for triblock copolymer melts in the experiments carried out by Cochran and Bates.[45] Since different cocontinuous network phases could in principle be obtained, the structure factor, $S(q)$, of the simulated network phase was calculated. Figure 4 shows different projections of the calculated $S(q)$. The location of the peaks is indeed consistent with the *Pnna* symmetry (i.e., the O^{52} phase) and with the $S(q)$ obtained by Cochran and Bates.[45] Moreover, simulations only produced a defect free O^{52} phase when the edges of the simulation box had sizes consistent with ratios about 2:b:1 with $b \sim 1.8-1.9$, which are comparable with the ratios observed experimentally for triblock copolymers (i.e., 2:1.73:1).[45] At this point it is important to note that even though additional simulations were carried out in boxes with dimensions consistent with the lattice constants of the O^{70} phase,[5] the latter was never observed. Finally, for high solvent concentration (i.e., $\phi_{\mathrm{add}} \sim 0.40$) the "reversed" perforated lamellae phase (RPL) and the "reversed" gyroid phase (RG) were observed. In the RPL phase the B blocks form perforated lamellae surrounded by an A-component (i.e., A blocks + solvent particles) matrix. Similarly, the RG phase presents B-component interweaving networks in an A-component matrix.

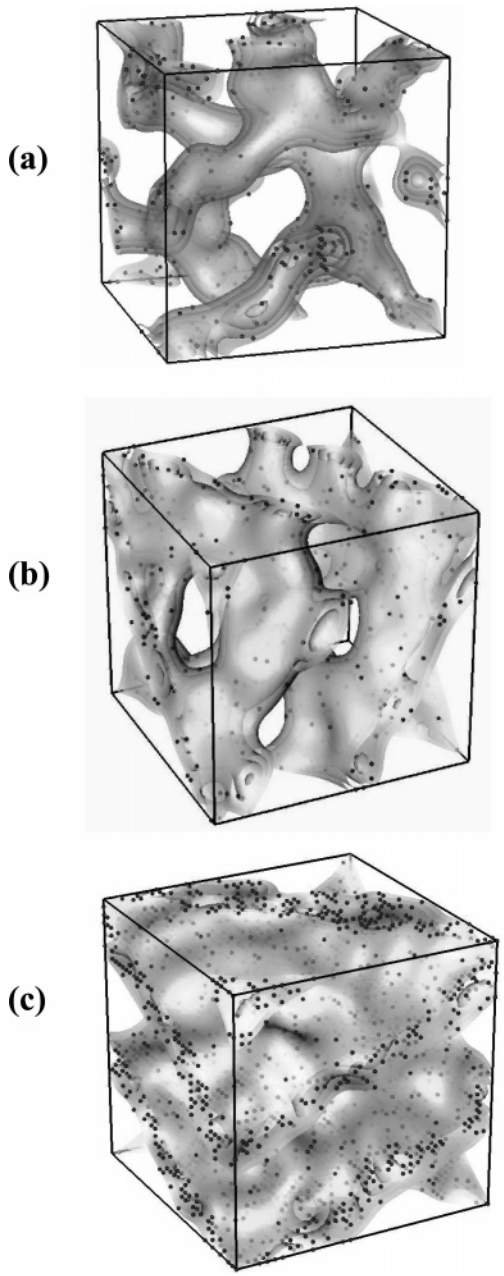

Figure 2. Commonly observed morphologies in DBC systems that were obtained by the addition of selective solvent particles. The majority (B) component is not shown. Solvent particles that are located in the majority component domain are not shown for clarity. (a) The G phase, (b) the PL phase, and (c) the L phase.

As pointed out in previous works,[20,21,23] the mesophases obtained in simulations of DBC melts are particularly sensitive to the choice of simulation box dimensions. As a consequence, at a given set of thermodynamic conditions more than one morphology can be observed. While the system DBC/solvent particles can no longer be considered a "melt", we still find the observed structures to be extremely sensitive to the choice of simulation box dimensions. Thus, the most stable phase has to be discerned by comparing the values of the chemical potentials as discussed in section III. In Figure 5, we present an approximate phase diagram where all the spontaneously obtained morphologies are shown as a function of the solvent concentration ϕ_{add}. Though several mesophases can be shown at a given ϕ_{add}, phase boundaries between the stable phases are roughly delineated on the basis of calculated values of βg. In general, the stable phases showed a progression of the form

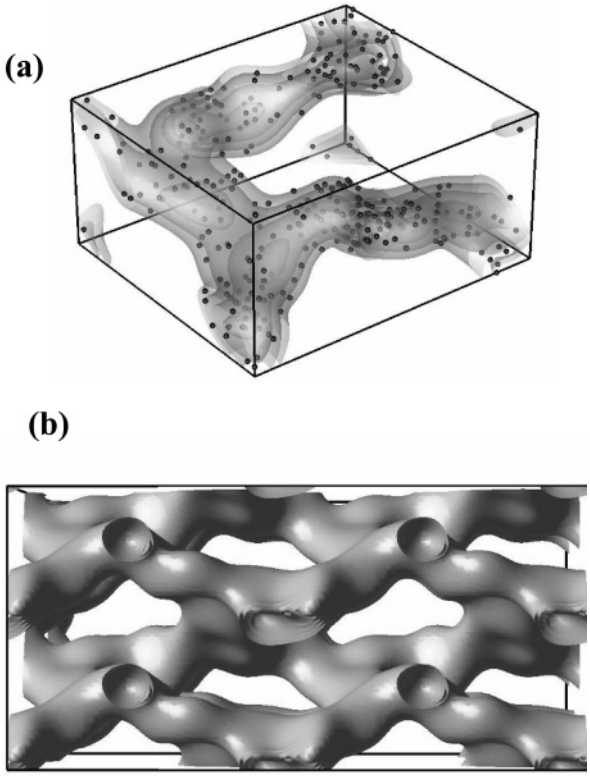

Figure 3. Orthorhombic cocontinuous network phase O^{52} observed in simulations for a solvent concentration range of $\phi_{add} \sim 0.05-0.09$. Solvent particles that are located in the majority component domain are not shown for clarity. (a) A unit cell of the O^{52} phase. (b) Eight (8) unit cells of the O^{52} phase.

G → PL → L → RG with increasing ϕ_{add}. Although the O^{52} phase was observed in the range $\phi_{add} = 0.05-0.09$, free energy calculations indicate that this phase is a long-lived metastable and that the stable phase in this region of the phase diagram is the PL phase [e.g., for $\phi_{add} = 0.06$, $\beta g^{O^{52}} = 17.57(1)$ and $\beta g^{PL} = 17.55(1)$]. However, the very small difference in molar Gibbs free energy between these two phases (i.e., PL and O^{52}) together with the fact that simulations are only carried out in discrete points of the phase diagram suggests that this result should be taken with caution; there could still be a very narrow region of the phase diagram where the O^{52} phase is stable. Moreover, the potential existence of the O^{52} phase as a long-lived metastable phase is also of interest since metastable phases are often observed in experiments (e.g., the PL phase in pure DBC melts[10]). In a similar note, at $\phi_{add} = 0.40$ the RG phase was observed in a cubic simulation box of size $L_{box} = 39$ lattice units, with a calculated value of Gibbs energy of $\beta g^{RG} = 4.595(2)$. In simulation boxes of sizes different than the latter, the RPL phase was always found. However the values of chemical potential for the RPL were always higher [e.g., $L_{box} = 35$, $\beta g^{RPL} = 4.600(2)$], indicating the stability of the RG phase in this point of phase diagram. (Note that at $\phi_{add} = 0.40$ the mole fraction of solvent particles is $y^{nano} \sim 0.93$, hence, the low values of the molar Gibbs energy of the mixture.)

Although the addition of selective solvent induced the formation of a variety of morphologies, neither the DD phase nor the P phase was observed. The reason for the absence of these phases can be explained in terms of spatial distribution of the solvent particles throughout the minority (A-component) domain. In order to achieve the stabilization of the bicontinuous phases, the solvent particles need to preferentially reside inside the nodes (Figure 1b). However, given the small size of the solvent particles, it is reasonable to think that confining the

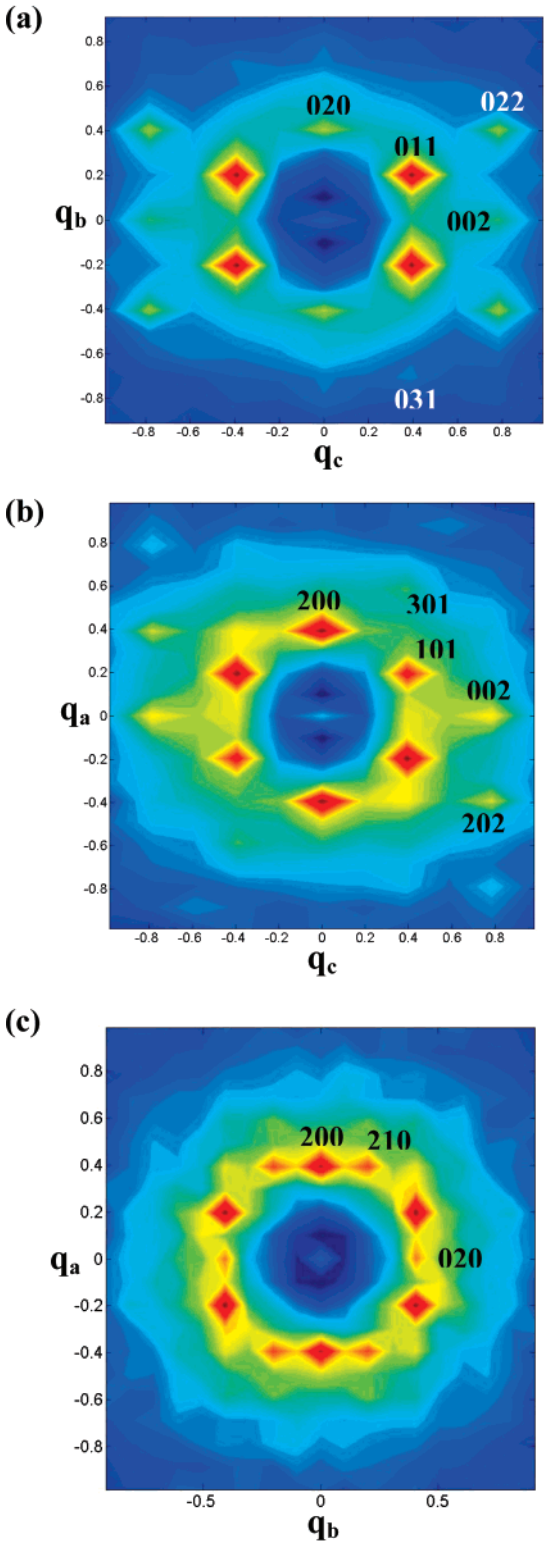

Figure 4. 2D projections of the structure factor for a simulated O^{52} phase with lattice constants $a = 32$, $b = 31$, and $c = 16$ (lattice units), obtained at a solvent concentration of $\phi_{add} = 0.06$. Location of peaks is consistent with the *Pnna* symmetry. (a) Projection in the "*a*" axis. (b) Projection in the "*b*" axis. (c) Projection in the "*c*" axis.

solvent to small regions (e.g., the nodes) of the A domain would produce a significant penalty to the entropy of mixing. Therefore, solvent particles would tend to distribute uniformly throughout the minority component domain. This tendency can be observed in Figure 6a, where we show a typical snapshot of the L phase with solvent concentration $\phi_{add} = 0.20$. Figure 6b shows the concentration profiles of A-block beads and solvent

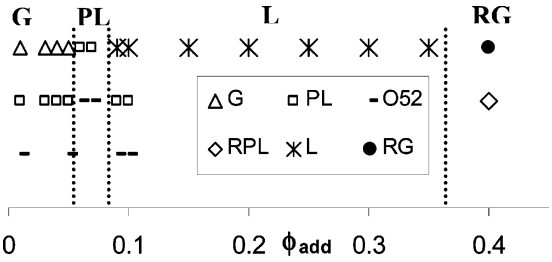

Figure 5. Approximate phase diagram where the morphologies obtained by addition of selective solvent particles are presented as a function of the solvent concentration ϕ_{add}. All the morphologies observed (i.e., stable and metastable) are shown. Approximate phase boundaries between stable phases—which are indicated in big bold letters—are based on the chemical potential calculations. A progression of the form G → PL → L → RG is observed with increasing ϕ_{add}.

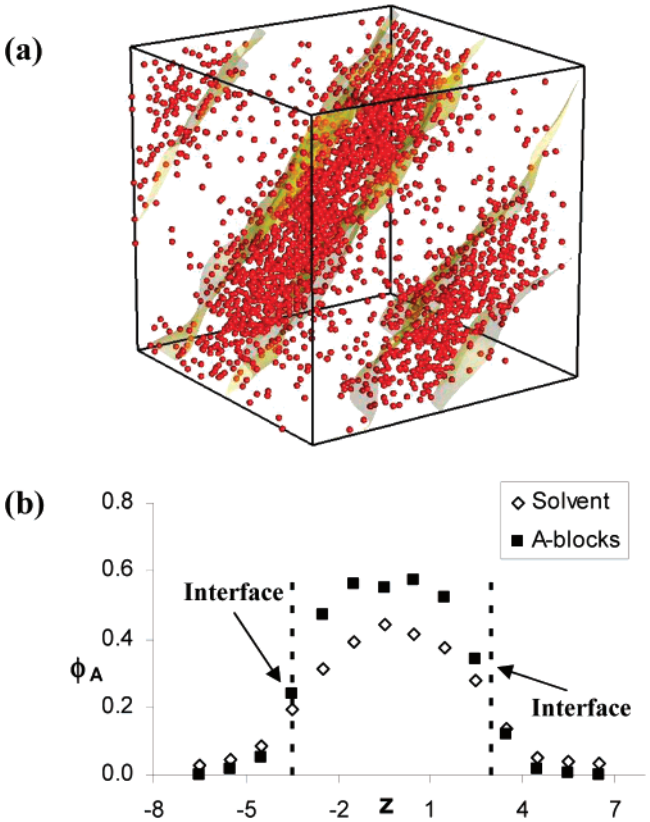

Figure 6. Distribution of selective solvent particles in simulated L phase at $\phi_{add} = 0.20$. (a) Typical snapshot of the simulated L phase. For clarity, copolymer beads are not shown. Solvent particles are shown in red (dark). Surfaces dividing the A and B domain are shown as a guide to the eye. (b) Concentration profiles along the direction perpendicular to the lamellae are shown for the A-block beads and solvent beads. Solvent particles concentration varies less rapidly than that of A-block beads, indicating that the solvent particles tend to distribute homogeneously throughout the A-component domain. Non-negligible amounts of solvent particles can also be found in the B-component domain. A similar behavior is observed (results not shown) for the other solvent-stabilized phases (e.g., G, O^{52}, PL, and RPL).

beads along the direction perpendicular to the Lamellae. The concentration of solvent particles is seen to vary less rapidly than the concentration of A-block beads as the interface is approached, consistent with the higher tendency of the solvent particles to distribute uniformly in the A domain. Moreover, as the interface is approached, the concentration of solvent beads increases relative to that of A-block beads to the point that solvent particles are also present in finite concentrations (despite the energetic penalty implied) inside the B-component domain.

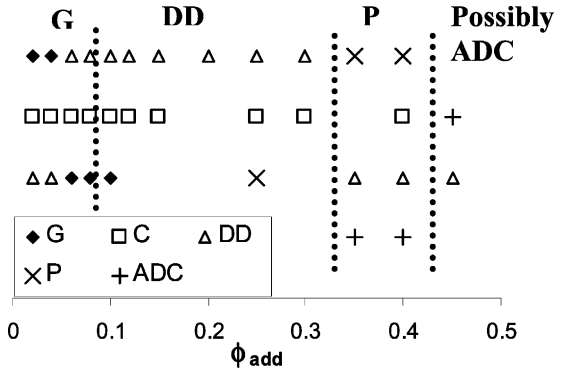

Figure 7. Simulated phase diagram for the DBC/homopolymer system. All the morphologies obtained at a particular value of ϕ_{add} are shown. Chemical potential calculations are used to discern stability between competitive phases and to delineate approximate phase boundaries. In general, a progression of morphologies G → DD→ P was observed. Also, a possibly stable morphology of "alternating diameter cylinders" (ADC) wherein cylinders pack tetragonally was observed at high ϕ_{add}.

This illustrates the importance of the solvent particle mixing entropy contribution to the total free energy. As a consequence, the small solvent particles studied in this work are not likely to locate preferentially inside the nodes of a bicontinuous phase, thereby failing to stabilize either the DD phase or the P phase through reduction of packing frustration. It is also instructive to note that since the solvent tends to distribute uniformly in the A-component domain, the net effect of adding solvent particles is to increase the effective size of the minority component block of the DBC (i.e., swelling the whole A-component block), hence decreasing the preferred mean curvature of the A−B interface. This is consistent with the observed progression of stable phases in which the system goes, with increasing ϕ_{add}, from the G phase (i.e., positive mean curvature) to the L phase (i.e., zero mean curvature), and then to the RG phase (i.e., negative mean curvature).

Addition of Homopolymer. In this section, we study the possibility of reducing packing frustration in the ordered bicontinuous phases by addition of A-component homopolymer of size $N_{ho} = 16$. The choice of this homopolymer size is a compromise between two opposite factors: (1) The smaller the homopolymer chains, the greater the mixing entropy penalty that is incurred in order to confine the homopolymer inside the nodes. Accordingly, longer homopolymer chains should favor the formation of bicontinuous phases. (2) The longer the homopolymer chains, the greater the dislike between the homopolymer and the DBC chains, thus increasing the tendency of macrophase separation into a DBC-rich phase and a homopolymer-rich phase; this hinders the possibility of obtaining multiple bicontinuous phases. Thus, our choice of homopolymer chain size is consistent with the SCFT calculations of Matsen[24] where it was found that these two criteria can be met, in order to stabilize the DD phase, when the ratio (α) of homopolymer chain length to DBC chain length is around $^2/_3 \leq \alpha \leq 1$.

The phase behavior of the DBC/homopolymer system was studied for values of homopolymer volume fraction (ϕ_{add}) in the range $\phi_{add} \sim 0.0-0.45$. A very complex phase behavior was observed, which is shown in Figure 7. As before, all the morphologies spontaneously formed for a given value of ϕ_{add} are shown. Phase boundaries between stable phases are roughly delineated on the basis of free energy calculations.

As expected, for low homopolymer concentration $\phi_{add} \sim 0.0-0.10$, the G phase was observed. In addition, for a wide range of concentrations $\phi_{add} \sim 0.00-0.40$ the C phase was obtained. For values of $\phi_{add} \geq 0.02$, the ordered bicontinuous DD phase

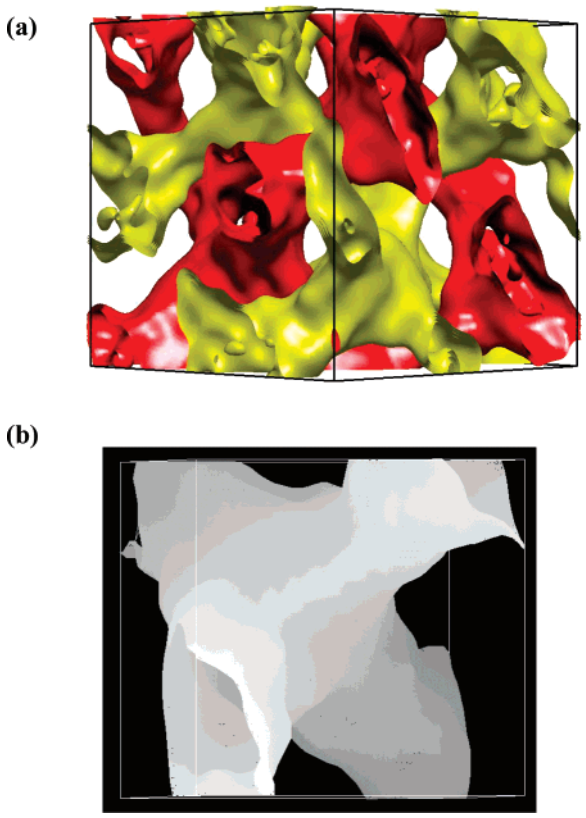

Figure 8. Snapshot of a simulated DD phase for the DBC/homopolymer system at $\phi_{add} = 0.20$. (a) Eight unit cells of the simulated DD phase (the unit cell size is $L = 30$ lattice units). The B-component domain is not shown for clarity. The two minority component networks are shown in red (dark) and yellow (light) for clarity. (b) A single DD node, where the four connectors are seen to intersect.

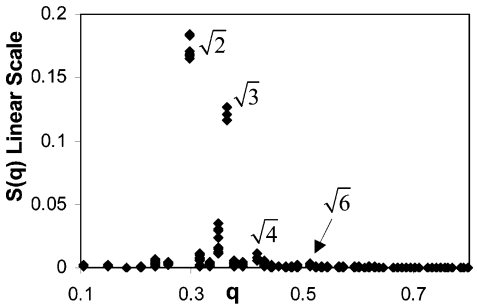

Figure 9. Structure factor $S(q)$ for the simulated DD phase. The location of the peaks at ratios $\sqrt{2}:\sqrt{3}:\sqrt{4}:\sqrt{6}$ is consistent with the *Pn*3*m* symmetry.

was also observed. In Figure 8a a snapshot of eight unit cells of the simulated DD phase is shown. As is customary throughout this work, the B-component domain is not shown. The minority (A) component forms two interweaving networks that never intersect. Figure 8b shows a single node of the simulated DD phase; as expected, four tubes (connectors) intersect in each node. In order to ratify the simulated morphology as the DD phase, the structure factor $S(q)$ was calculated (Figure 9) to show that the location of the peaks at ratios $\sqrt{2}:\sqrt{3}:\sqrt{4}:\sqrt{6}$ is indeed consistent with the DD phase (i.e., *Pn*3*m* symmetry). To the best of our knowledge, this constitutes the first time the DD phase is successfully obtained in particle-based simulations in DBC systems and at meltlike densities.

Since the DD has periodicity in the three directions, its formation is very sensitive to the simulation box dimensions. As consequence, the DD phase was only observed when

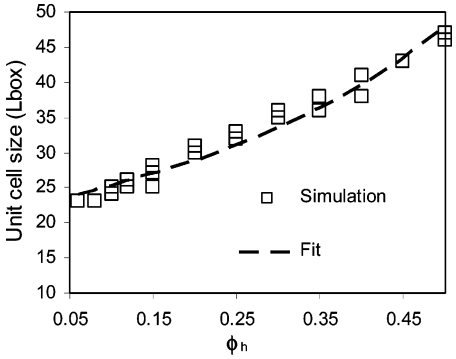

Figure 10. Simulation box dimensions (of one unit cell), wherein the DD phase was spontaneously formed, as a function of the homopolymer volume fraction $\phi_h = \phi_{add}$. A single-parameter (λ) fit using eq 11 is also shown. The fitted value of $\lambda = 4.45$ represents the half-width of the B-component domain.

simulation boxes were consistent with the DD unit cell size, which is a function of the thermodynamic conditions. For simulations with box dimensions inconsistent with the preferred DD unit cell size, other phases (e.g., C, G, etc.) were formed depending on the value of ϕ_{add}. This dependence on simulation box dimensions of the observed structure is a general difficulty of particle-based simulations of all the ordered bicontinuous phases, since the "appropriate" unit cell size for each morphology at a given point of the phase diagram is not known a priori. Thus, in principle, an extremely large number of simulation box sizes (and shapes in the case of orthorhombic phases) would need to be tried to be able to observe all the competitive morphologies. This approach is obviously not feasible, and physical intuition together with some degree of trial-and-error process is necessary to constrain the search to only simulation box sizes consistent with the morphologies that are most likely to have the lowest free energy. In order to estimate the unit cell size of the different candidate morphologies from data obtained at a different value of ϕ_{add} or from another bicontinuous morphology, we found it helpful to use simplified theoretical models for the geometry of bicontinuous phases. The simplest physical model to represent ordered bicontinuous phases is the "constant thickness" or "parallel surfaces" model,[4,16] in which the A−B interfaces are assumed to lie at a constant perpendicular length λ from the minimal surface (e.g., G, DD, P surfaces) which is imagined to divide the B-component domain in two halves. In this model, the B-component volume fraction ϕ_B is related to length λ by the simple relation:[16]

$$\phi_B = 2A_0\left(\frac{\lambda}{L}\right) + \frac{4\pi\chi_e}{3}\left(\frac{\lambda}{L}\right)^3 \qquad (11)$$

where L is the preferred unit cell size and A_0 and χ_e are the normalized area per unit cell and the Euler characteristic, respectively, for the particular minimal surface. For the DD phase $A_0 = 1.919$ and $\chi_e = -2$; while for the P phase, $A_0 = 2.345$ and $\chi_e = -4$.[16] The first term of eq 11 corresponds to the value that ϕ_B would be if the minimal surface were flat (i.e., Gaussian curvature $K = 0$) and the second term to the correction due to the nonzero value of K. In Figure 10, we show the simulation box sizes where the DD phase was spontaneously obtained as a function of the homopolymer volume fraction ϕ_{add}, which is related to ϕ_B through

$$\phi_B = 1 - \phi_A = 1 - [f(1 - \phi_{add}) + \phi_{add}] \qquad (12)$$

where $f = 0.30$ is the DBC composition. Additionally, Figure 10 shows the fit provided by eq 11 with a single adjustable parameter λ that represents the half-width of the B-component domain. For the DD phase we found $\lambda = 4.46$ lattice units, which is about 0.75 times the observed B-block end-to-end distance (r_B) for the DD phase and agrees with the intuitive idea that the width of the B domain should lie in between those expected for a monolayer and a bilayer (i.e., $r_B/2 < \lambda < r_B$). Similar values of λ were obtained for the G phase (e.g., $\lambda = 4.32$) and the P phase (e.g., $\lambda = 4.52$), indicating that the B-component domain width is almost independent of the bicontinuous morphology. It can be seen in Figure 10 that the simulation box size dependence in ϕ_{add} agrees well with the expected behavior for the constant thickness model of the DD phase. A similar analysis was performed for the other bicontinuous phases encountered in our simulations, and a similar degree of agreement with eq 11 was also observed (results not shown). Moreover, the good agreement between the simulation results and eq 11 indicates that λ remains approximately constant for the different values of ϕ_{add}. This trend can only be explained if the homopolymer does not penetrate into the B-component domain, a behavior that we have indeed observed in our simulations (see later the discussion on Figure 16).

In the range $0.02 \le \phi_{add} \le 0.40$ both the DD phase and the C phase were spontaneously obtained depending upon simulation box size. For $\phi_{add} < 0.05$ both of these phases are just metastable since the G phase has lower values of Gibbs energy [e.g., at $\phi_{add} = 0.04$, $\beta g^G = 35.70(1)$, $\beta g^C = 35.76(1)$, and $\beta g^{DD} = 35.81(1)$]. However, for the range $0.05 < \phi_{add} < 0.35$ the DD and C phases seem to compete for thermodynamic stability. For relatively high concentrations of homopolymer (i.e., $\phi_{add} > 0.12$) the Gibbs energy of the DD phase is found to be slightly lower than that of the C phase [e.g., for $\phi_{add} = 0.25$, $\beta g^{DD} = 32.597(9)$ and $\beta g^C = 32.62(1)$]. Additionally, for these concentrations, defect-free C phases become increasingly difficult to stabilize, thus making unambiguous the assignment of the DD phase as the stable one. However, for a narrow range of homopolymer concentrations (i.e., $0.05 < \phi_{add} < 0.12$), free energy calculations seem to indicate that the C phase has a lower Gibbs energy than the DD phase [e.g., for $\phi_{add} = 0.08$ and $L_{box} = 48$, $\beta g^{DD} = 35.175(10)$ and $\beta g^C = 35.15(1)$]. The stabilization of the C phase (a phase with much greater mean curvature in the A−B interface than the G phase) with the addition of homopolymer is somewhat counterintuitive. However, this could be the consequence of an incomplete alleviation of the frustration in the DD nodes because of the relatively small amounts of homopolymer present in this region of phase diagram (i.e., $0.05 < \phi_{add} < 0.12$). Nonetheless, to the best of our knowledge, a similar transition (i.e., from the G phase to the C phase by adding minority component) has neither been observed experimentally nor predicted by theory. It is also plausible that the stable state in this narrow region of phase diagram is a two-phase state where the G and DD phases coexist, which would not be attainable in the relatively small simulation boxes used in this work, therefore causing the stabilization of a single metastable phase which in this case happens to be the C phase. Moreover, the C morphologies with the lowest Gibbs energy were usually the ones with the cylinders aligned along a diagonal of the simulation box. This suggests that C configurations are subject to "tensions" (i.e., anisotropies in the pressure tensor) that could cause a nonnegligible penalty in the PV contribution to the Helmholtz free energy. Because of the above reasons, in this region of the phase diagram, we tentatively assign the C phase as metastable. Finally, to estimate the phase boundary between the two stable phases in this region, we show in Figure 11 the Gibbs free energy of the G and DD phases as a function

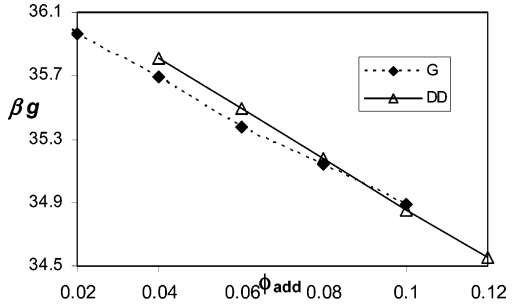

Figure 11. Gibbs free energy of the mixture (βg) for the G and DD phases in the DBC + homopolymer system as a function of the homopolymer volume fraction ϕ_{add} in the range $\phi_{add} \sim 0.02-0.12$. The G phase is stable only for $\phi_{add} < 0.09$.

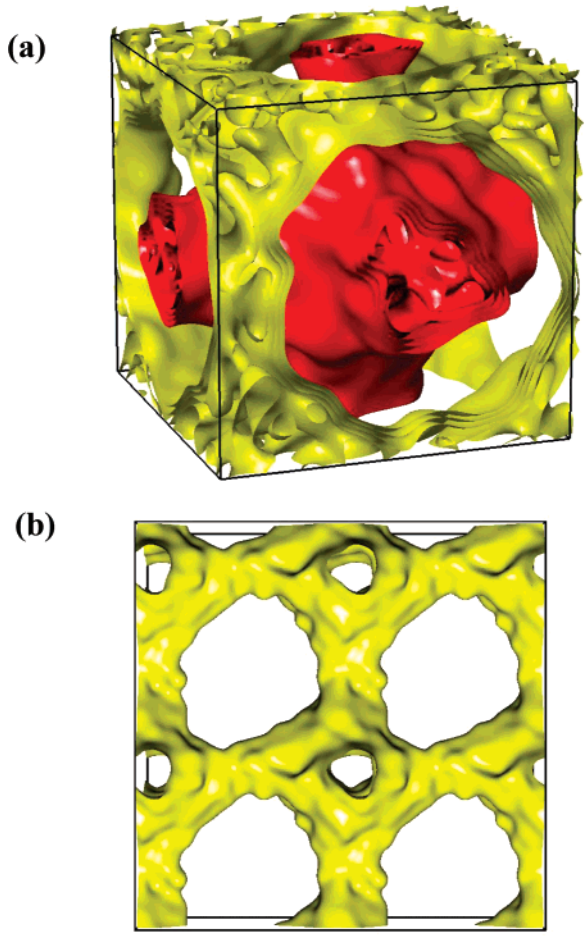

Figure 12. Simulated snapshot of the plumber's nightmare (P) phase observed at $\phi_{add} = 0.35$ in a simulation box of size $L_{box} = 46$. The majority (B) component is not shown. (a) One unit cell of the P phase. The minority component forms two distinct networks that never intersect. They are shown in yellow (light) and red (dark) for visualization purposes. (b) One of the minority component networks has been replicated four times.

of ϕ_{add}, wherein it can be seen that the values of βg for these phases intersect around $\phi_{add} \sim 0.09$.

For homopolymer volume fractions in the range $0.25 < \phi_{add} < 0.40$ the plumber's nightmare (P) phase was also observed. To the best of our knowledge, this phase has never been observed before in simulations of DBC systems. In this morphology, the minority component forms two networks that never intersect, and each network is composed of 6-fold nodes and connectors (Figure 12). Calculation of $S(q)$ in Figure 13 confirms that the simulated phase is indeed the P phase (i.e., *Im*3*m* symmetry)[25] as can be seen from the clear peaks at

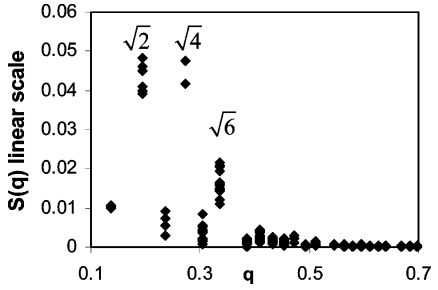

Figure 13. Structure factor $S(q)$ for the simulated P phase. The location of the peaks at ratios $\sqrt{2}:\sqrt{4}:\sqrt{6}$ is consistent with the *Im*3*m* symmetry that is expected for the plumber's nightmare phase.

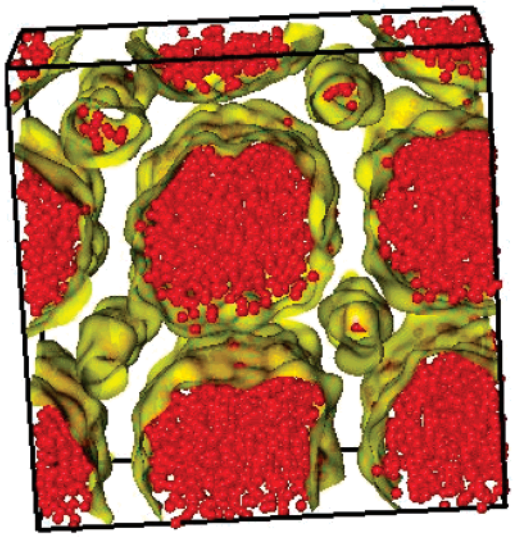

Figure 14. Simulated snapshot of four unit cells of the "alternating diameter cylinder" (ADC) phase. The majority component is not shown. The A−B interface is shown in yellow (light), while the centers of mass of the homopolymer chains are shown in red (dark). This snapshot was obtained at $\phi_{add} = 0.40$ where the unit cell size is $L = 39$. The interior of the "thick" cylinders is rich in homopolymer chains, while the interior of the "thin" cylinders present a much lower homopolymer concentration. Cylinders pack tetragonally.

positions $\sqrt{2}:\sqrt{4}:\sqrt{6}$. For homopolymer concentrations $\phi_{add} \leq 0.30$ the simulated P phases became defective after long simulation runs (i.e., more than 4×10^6 MC steps), indicating that for these conditions the P phase is just metastable. However, in the range $0.35 \leq \phi_{add} \leq 0.40$ the simulated P phase not only remained defect free but additionally was observed to have a slightly lower Gibbs energy than the DD phase [e.g., for $\phi_{add} = 0.35$, $\beta g^{DD} = 31.19(1)$ and $\beta g^{P} = 31.18(1)$]. Moreover, when "bigger" systems were used (e.g., at $\phi_{add} = 0.40$, box dimensions of $41 \times 82 \times 82$ for the DD phase and $49 \times 98 \times 98$ for the P phase), such that the unit cells of the P and DD phases were replicated four times, the P phase still showed lower values of βg. As a consequence, we conclude that in the range $0.35 < \phi_{add} < 0.40$ the P phase is the stable phase.

For homopolymer volume fractions $\phi_{add} > 0.35$, a novel phase, in which cylinders of two different diameters alternate in a tetragonal (square) packing, was observed (Figure 14). This phase will be, henceforth, referred to as "alternating diameter cylinders" (ADC). Although chemical potential calculations in the range $0.35 < \phi_{add} < 0.40$ indicate that the ADC phase is just a long-lived metastable phase, the results seem to suggest that for $\phi_{add} \sim 0.45$ the ADC phase may be stable since it has a lower chemical potential than the other phases observed. However, this result should be taken with caution because most of the other phases observed at these conditions were defective,

presumably because of the much longer equilibration times required for the large simulation boxes involved (e.g., at $\phi_{add} = 0.45$ $L_{box} > 51$ for the P phase). Moreover, at these high values of ϕ_{add} it is also possible that other bicontinuous phases [e.g., C(P), I−WP, etc.[16]] could become stable. These phases, however, would have unit cell sizes far beyond those accessible in the present study [e.g., at $\phi_{add} = 0.45$, $L_{box} \sim 80$ for the Neovius' surface phase estimated with eq 11] and are outside the scope of the present work. Nevertheless, even in the worst case scenario wherein the ADC phase is just a long-lived metastable, we still think this phase is of significant importance for several reasons: (1) long-lived metastable phases are often observed experimentally, (2) under different conditions (e.g., different thermodynamic conditions, different model, or when subject to shear) this phase might be stabilized, and (3) the fact that the cylinders are arranged in a tetragonal packing gives insight about why the "ordinary" C phase is not stable in this region of the phase diagram. At high values of ϕ_{add}, if all the cylinders had the same diameter, packing frustration of the B-block would be prevalent in the corners of the Wigner−Seitz cell of the hexagonally packed cylinders. This is because the mean end-to-end distance of the B-blocks would be much smaller than the radius of the cylinders. This is evident in Figure 14 where it can be readily seen that the average B-domain distance separating two consecutive cylinders is much less than the diameter of the thick cylinders. It is interesting to note that the penalty in mixing entropy incurred by segregating the homopolymer in this way (i.e., having homopolymer-rich cylinders and DBC-rich cylinders) seems to be outweighed by the gain in conformational entropy of the B-block.

At high values of ϕ_{add}, and for the homopolymer relative length studied here, the SCFT calculations of Matsen[24] predict that macrophase separation in a DBC-rich phase and a homopolymer-rich phase should occur. Though those calculations were carried out at values of segregation much lower (i.e., $\chi N < 24$) than the value used in this work (i.e., $\chi N = 40$) and do not take into account finite chain-length effects, it is possible that the stable state for high values of ϕ_{add} is a state of phase coexistence which could not be attained given the relatively "small" simulation box sizes used in this work. However, no signs of any such (partial) phase separation was observed in the simulation snapshots examined, not even for the largest boxes tested (e.g., in a 49 × 98 × 98 box).

It has been argued that the reason for the lack of multiple ordered bicontinuous phases in pure DBC melt systems is the presence of packing frustration inside the nodes, which can be manifested in the form of void in the nodal centers,[20] chain stretching,[21] deformation of the nodes shape,[19] or more likely a combination of all the above factors. We have now shown here that by the addition of a component with the right characteristics, multiple bicontinuous phases (e.g., DD and P phases), can be stabilized. In order to link this stabilization to reduction in the packing frustration inside the nodes, we show in Figure 15a a single node of a typical snapshot of the simulated P phase, where the A−B interface in yellow (light) has been made transparent in order to show the centers-of-mass of the homopolymer chains in red(dark). Additionally, Figure 15b shows a plot of the volume fraction of the A-block and homopolymer beads as a function of the distance from the center of the P phase nodes. It can be seen from the figure that the homopolymer chains reside preferentially inside the nodes where they are found in much higher concentration (i.e., $\phi \sim 1.0$) than in the connectors. Moreover, since the concentration of DBC chains in the center of the nodes is essentially zero, the absence of the homopolymer

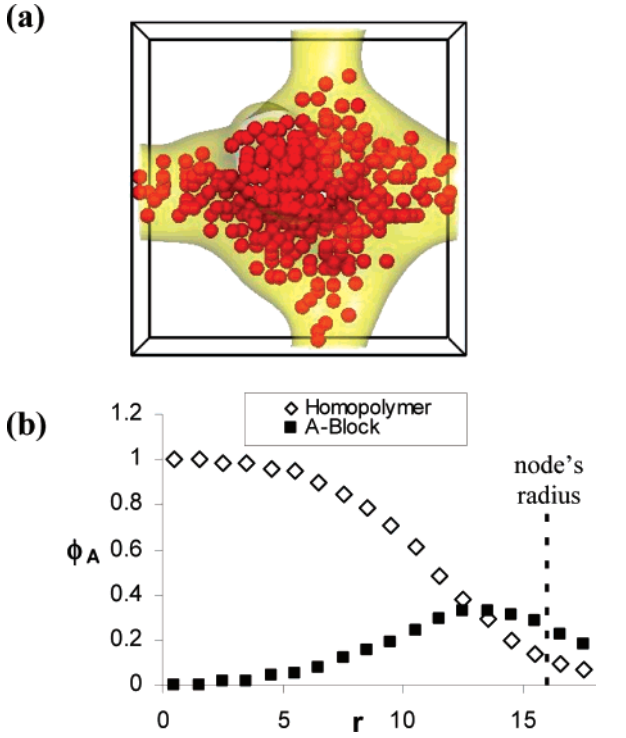

Figure 15. Typical snapshot of a single node of the P phase obtained at $\phi_{add} = 0.25$ and $L_{box} = 41$. (a) The A−B interface in yellow (light) is made transparent and the centers of mass of the homopolymer chains are shown in red (dark). (b) Average volume fraction of homopolymer beads and A-block beads as a function of the distance from the nodes. The homopolymer chains concentrate in the center of the node in order to reduce packing frustration. A similar behavior was observed in all the snapshots we examined.

chains would clearly cause packing frustration because the DBC chains would need to stretch and the node would have to deform in order to diminish the void in the center of the nodes. A similar behavior is observed for the DD phase (results not shown); however, for a given value of ϕ_{add} the segregation toward the nodes of the homopolymer chain is more dramatic in the case of the P phase than in the DD phase. This is consistent with the hypothesis that since the P nodes are bulkier (e.g., at $\phi_{add} = 0.25$, $r_{node} \sim 16$ for the P phase and $r_{node} \sim 12$ for the DD phase), the DBC packing frustration would be more drastic for the P phase if there were no homopolymer inside the nodes. Although a gradient of homopolymer concentration implies a loss of mixing entropy, yet again, for this size of homopolymer, the gain in conformational entropy for the DBC chains seems to partially outweigh this loss. Moreover, analysis of the mean square end-to-end distance $\langle r^2 \rangle$ of the homopolymer chains inside and outside the nodes [e.g., $\langle r^2 \rangle_{tube} = 29.5(9)$ and $\langle r^2 \rangle_{node} = 35.5(9)$], and comparison with the $\langle r^2 \rangle$ observed in a melt of the pure homopolymer [e.g., $\langle r^2 \rangle_{melt} = 35.3(1)$] reveals that the homopolymer in the tubes is forced to adopt unfavorable, more compact conformations (due to the smaller size of the tubes relative to the nodes). This indicates that the segregation of the homopolymer toward the nodes may also be understood from the perspective of the homopolymer sacrificing translational entropy in order to gain conformational entropy, which (for this hompolymer length) is expected to have a larger impact on the total free energy.

Discussion on the Origins of Complex Phase Behavior. Although it is clear that reduction of chain stretching inside the bicontinuous phases' nodes (frustration relief) by addition of homopolymer should make these morphologies less unfavorable, it certainly does not guarantee that these phases should

become the stable ones, as observed in this work. Moreover, packing frustration alone cannot explain the complex progression of phases observed with increasing ϕ_{add} because just as the homopolymer reduces the frustration in the DD phase so does it in the G phase, and there would not be any driving force for phase transitions to occur.

In order to understand the observed phase transitions, it is convenient to evoke the origins of curvature in the DBC systems. The morphologies observed in DBC systems are the result of the competition between energetic and entropic contributions to the free energy. In order to decrease the interfacial energy, the system tries to approach morphologies of zero mean A−B interface curvature (H); however, if the two blocks are of different sizes, imposing $H = 0$ forces the blocks to adopt unfavorable configurations in order to fill space, creating an entropically unfavorable scenario (i.e., packing frustration). Thus, the resulting equilibrium morphology possesses an A−B interface that *tries* to approach a constant mean curvature surfaces (CMC). The preferred value of mean curvature (H^{pre}) depends upon the relative size of the two blocks as is observed in the pure DBC system where the curvature of the interface is progressively increased with the asymmetry of the two blocks, going from the L phase (i.e., $H = 0$) when the blocks are symmetric, to the S phase, with a high value of H, when the blocks are highly asymmetric.

For a specific relative size of the blocks in a DBC chain (i.e., for a given value of f) the preferred value of H can be modified by adding a second component that "likes" the minority component blocks. For example, as we showed above, adding selective solvent particles can induce a variety of structures with different values of H because the small solvent particles, driven by their high entropy of mixing, distribute almost homogeneously in the A-component domain, causing the swelling of the A-blocks and thus increasing their effective size. In other words, since the solvent particles "penetrate" into the DBC layer, the net effect of adding them is akin to increasing the A-block size. Conversely, if the selective "additive" does not penetrate into the DBC layer, the A-blocks will not augment their effective size and the preferred value of H will remain mostly unchanged. Whether an additive distributes homogeneously inside the A-component domain or not is again a competition between energetic and entropic terms.[2] The interfacial energy tends to "push" the additive away from the interface, concentrating the additive in the center of the A-domain. The entropy of mixing tends to favor configurations wherein the additive is spatially distributed in a uniform fashion. For the selective solvent particles the entropic contributions tend to outweigh the energetic ones causing their penetration into the DBC layer. However, for the homopolymer chains used in this study, the total entropy does not primarily arise from translational degrees of freedom (as with the solvent), but mainly from the chain conformations. The homopolymer can then be expected to have a much lower entropy of mixing (associated with the translational degrees of freedom), so that the energetic contributions should be dominant and the homopolymer chains should not significantly penetrate the DBC layer. This is indeed what is seen in the simulations. Figure 16a shows a typical snapshot of the C phase, where the centers of mass of the homopolymer chains are represented by the red (dark) beads, while the centers of mass of the A-blocks are presented in yellow (light). Figure 16b presents the volume fraction of homopolymer beads and A-block beads as a function of the distance from the cylinder axis. The homopolymer significantly concentrates in the center of the cylinders while most of the A-blocks just surround the

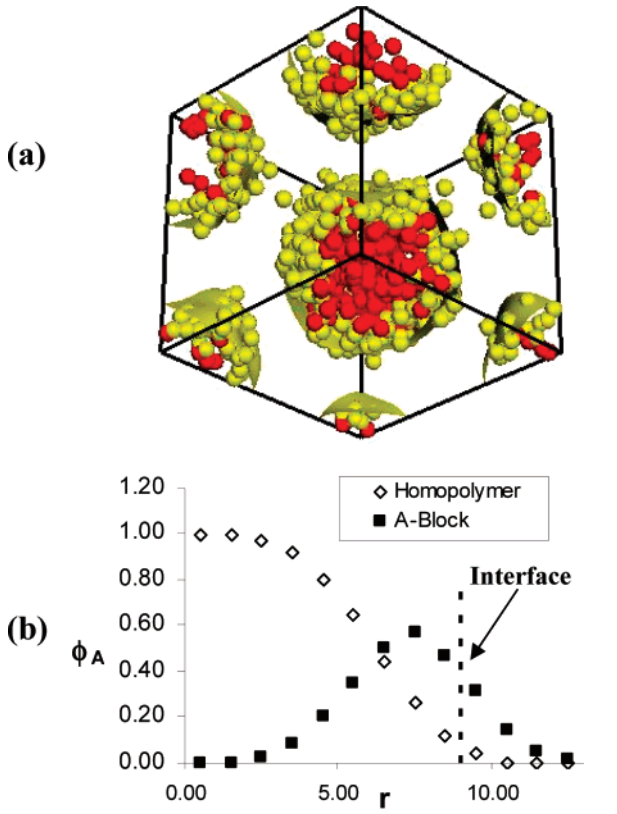

Figure 16. Typical snapshot of a metastable C phase observed at $\phi_{add} = 0.25$. The C phase offers a valuable opportunity to observe the inhomogeneous distribution of the homopolymer chains throughout the A-component domain. (a) The centers of mass of the A-blocks of the DBC chains are shown by the yellow (clear) beads, while the centers of mass of the homopolymer chains are represented by the red (dark) beads. The A−B interface is also shown in yellow (clear) for reference. (b) Average volume fraction of homopolymer beads and A-block beads as a function of the distance from the cylinder axis. The homopolymer does not distribute uniformly but prefers the center of the A-component domain.

homopolymer. Though this effect is most easily visualized in the C phase, the same trend is observed for all the other phases. Finally, we can postulate that, given that the homopolymer does not significantly penetrate the DBC layer, adding homopolymer should not significantly decrease the preferred value of H.

For a given morphology the actual value of the A−B mean curvature (H^{act}) can be estimated using the parallel surface model, for which it can be shown that[16]

$$H^{act} \approx (\phi_B)^2/\gamma\lambda \tag{13}$$

where γ is dimensionless constant particular to each minimal surface and λ represents the half-width of the B-component domain which is found to remain approximately constant (cf. eq 11 and discussion thereof). From this relation, it is seen that for a given morphology the actual value of the interfacial curvature is proportional to the square of the B-component volume fraction ϕ_B (and ϕ_B decreases as ϕ_{add} increases; cf. eq 12). Adapting the argument that Ström and Anderson[16] used to explain the phase behavior of surfactant systems to the case of DBC melts, we postulate that the stable morphology is going to be the one that, while minimizing packing frustration, presents an *actual* value of the interfacial mean curvature (H^{act}) that is the closest possible to the *preferred* value H^{pre}.

At this point, we get to the root of the origin of the contrasting difference between the phase behavior observed when adding

solvent particles and when adding homopolymer: the addition of solvent particles significantly decreases H^{pre} while the addition of homopolymer leaves H^{pre} mostly unchanged. For any selective additive, it is expected that the degree of penetration should increase with the additive concentration (i.e., because of the higher gradients); hence, H^{pre} should always decreases with additive concentration.[16] However, it is the difference in the rate at which H^{pre} decreases, which causes the contrasting phase behavior observed in the two types of systems studied. If the value of H^{pre} decreases *faster* than H^{act} with increasing concentration of additive (e.g., solvent case), the system progresses toward phases of less curvature. Conversely, if H^{pre} decreases slower than H^{act} with increasing concentration of additive (e.g., homopolymer case), the system progresses toward phases of more curvature.

The complex phase behavior observed with the addition of homopolymer can be now understood in terms of our postulate. First, let us establish that for a given value of ϕ_{add} the candidate phases can be sorted in the following manner with increasing curvature:[16] G → DD → P → C(P) → C. For small values of ϕ_{add} the system is just a slightly perturbed from the pure system and the G phase is stable. However, when the value of ϕ_{add} starts to increase, H^{act} decreases rapidly, departing from H^{pre} which stays approximately constant, therefore causing the G phase to become unstable. In order to approach a value of mean curvature closer to H^{pre} the system needs to undergo a phase transition to a new morphology of higher curvature. The next morphology in the list is the DD phase which, given the presence of the homopolymer and its tendency to concentrate in the nodes, is no longer limited by packing frustration and is therefore stabilized. When more homopolymer is added, H^{act} continues to decrease until again it departs significantly from H^{pre} and the P phase, whose frustration has again been relieved by the significant amounts of homopolymer added, becomes stable. As even more homopolymer is added, new phase transitions are expected to occur. The next phase in the list is the C(P) phase which as mentioned above would have unit cell sizes too large to be observed in the present study. Nevertheless, it is indeed observed that for high values of ϕ_{add} the ADC phase which presents a highly curved A−B interface spontaneously forms, consistent with the postulate of stabilization of phases of increasing curvature. As pointed out before, for high homopolymer concentrations, packing cylinders hexagonally as required for the C phase causes packing frustration in the B-blocks. Therefore, it is natural to assume that the stabilization of the ADC phase could be the result of a compromise between the system's need to achieve a highly curved interface like in the C phase and at the same time minimize packing frustration.

V. Conclusions

We performed a lattice MC study of two different strategies for reducing packing frustration in the ordered bicontinuous phases' nodes by means of the addition of minority (A) component. While the first strategy consisted of the addition of selective solvent particles, the second strategy involved addition of homopolymer of a length 80% that of the DBC chains.

The addition of solvent particles induced a progression of phases of the form G → PL → L → RG, in which the A−B interface curvature is observed to decrease monotonically with increasing solvent volume fraction (ϕ_{add}). Additionally, in the same region of phase diagram where the PL phase was found stable, the orthorhombic cocontinuous network O^{52} phase was observed, albeit as a long-lived metastable.

A radically different phase behavior was observed with the addition of homopolymer, in which phases of greater curvature than the G phase were stabilized. In general, the observed sequence of phases, for increasing homopolymer concentration, was G → DD → P, with the novel ADC phase being possibly stable after the P phase. To the best of our knowledge, this is the first time that the ordered bicontinuous DD and P phases are simulated and predicted to be stable in DBC melt systems using particle-based simulations. Examination of the structure of the ordered bicontinuous phases showed that the homopolymer preferentially locates in the center of the nodes, not only preventing the packing frustration that would otherwise exist but additionally allowing for a gain in homopolymer's conformational entropy.

The contrasting phase behavior observed for the two strategies was explained in terms of their difference in the rate of change of H^{act} relative to H^{pre} with increasing additive concentration. This difference originates from the disparity in degree of penetration of the two additives into the DBC layer, which ultimately originates in the difference in translational (mixing) entropy between the homopolymer and the solvent particles. It is interesting to note that for the currently studied system the DD phase is stable for an extraordinarily wide range of homopolymer concentrations (i.e., $0.09 < \phi_{add} < 0.30$). This suggests that the homopolymer length adopted here leads to a degree of penetration (into the DBC layer) which is to some extent "optimal" to stabilize the DD phase. Thus, it can be envisioned that "optimal" sizes of additive can be found for which the composition range of stability of a particular bicontinuous phase is maximized.

A limitation of the current work is the relatively short length of the simulated DBC chains, whose reduced conformational entropy could be leading to a more complex phase behavior than what could be attainable with high molecular weight DBCs. In the future, we plan to examine the effect of the DBC chain length on the appearance of selected bicontinuous phases. Additionally, future work will also be devoted to explore the possibility of provoking transitions between different complex phases by rationally controlling the additive's mixing entropy (and hence its degree of penetration into de DBC layer) through changes in the additive's architecture and chain length, while keeping constant the additive's volume fraction.

Acknowledgment. We are grateful to Professors Eric W. Cochran and Frank S. Bates for providing visualization models of the O^{52} and O^{70} phases. We also thank Professor U. Wiesner for stimulating conversations and for introducing us to the issues associated with the stabilization of the P phase in block copolymer−inorganic hybrid systems. The support by the US Department of Energy, Grant No. DE-FG02-05ER15682, is gratefully acknowledged.

References and Notes

(1) Hamley, I. W. *The Physics of Block Copolymers;* Oxford University Press: New York, 1998.
(2) Lin, Y.; Boker, A.; He, J. B.; et al. *Nature (London)* **2005**, *434*, 55.
(3) Matsen, M. W.; Schick, M. *Macromolecules* **1994**, *27*, 4014.
(4) Hajduk, D. A.; Harper, P. E.; Gruner, S. M.; et al. *Macromolecules* **1994**, *27*, 4063.
(5) Tyler, C. A.; Morse, D. C. *Phys. Rev. Lett.* **2005**, *94*.
(6) Takenaka, M.; Wakada, T.; Akasaka, S.; et al. *Macromolecules*, in press.
(7) Knoll, A.; Lyakhova, K. S.; Horvat, A.; et al. *Nat. Mater.* **2004**, *3*, 886.
(8) Schultz, A. J.; Hall, C. K.; Genzer, J. *J. Chem. Phys.* **2002**, *117*, 10329.
(9) Matsen, M. W.; Griffiths, G. H.; Wickham, R. A.; et al. *J. Chem. Phys.* **2006**, *124*.

(10) Hajduk, D. A.; Takenouchi, H.; Hillmyer, M. A.; et al. *Macromolecules* **1997**, *30*, 3788.
(11) Matsen, M. W. *Phys. Rev. Lett.* **1998**, *80*, 201.
(12) Andersson, S.; Hyde, S. T.; Larsson, K.; et al. *Chem. Rev.* **1988**, *88*, 221.
(13) Uehara, H.; Yoshida, T.; Kakiage, M.; et al. *Macromolecules* **2006**, *39*, 3971.
(14) Kamperman, M.; Garcia, C. B. W.; Du, P.; et al. *J. Am. Chem. Soc.* **2004**, *126*, 14708.
(15) Cho, B. K.; Jain, A.; Gruner, S. M.; et al. *Science* **2004**, *305*, 1598.
(16) Strom, P.; Anderson, D. M. *Langmuir* **1992**, *8*, 691.
(17) Hajduk, D. A.; Harper, P. E.; Gruner, S. M.; et al. *Macromolecules* **1995**, *28*, 2570.
(18) Matsen, M. W.; Bates, F. S. *J. Chem. Phys.* **1997**, *106*, 2436.
(19) Matsen, M. W.; Bates, F. S. *Macromolecules* **1996**, *29*, 7641.
(20) Martinez-Veracoechea, F. J.; Escobedo, F. A. *Macromolecules* **2005**, *38*, 8522.
(21) Martinez-Veracoechea, F. J.; Escobedo, F. A. *J. Chem. Phys.* **2006**, *125*.
(22) Hasegawa, H.; Hashimoto, T.; Hyde, S. T. *Polymer* **1996**, *37*, 3825.
(23) Dotera, T. *Phys. Rev. Lett.* **2002**, *89*.
(24) Matsen, M. W. *Macromolecules* **1995**, *28*, 5765.
(25) Finnefrock, A. C.; Ulrich, R.; Toombes, G. E. S.; et al. *J. Am. Chem. Soc.* **2003**, *125*, 13084.
(26) Jain, A.; Toombes, G. E. S.; Hall, L. M.; et al. *Angew. Chem., Int. Ed.* **2005**, *44*, 1226.
(27) Matsen, M. W. *J. Phys.: Condens. Matter* **2002**, *14*, R21.
(28) Fredrickson, G. *The Equilibrium Theory of Inhomogeneous Polymers*; Oxford University Press: New York, 2006.
(29) Fredrickson, G. H.; Ganesan, V.; Drolet, F. *Macromolecules* **2002**, *35*, 16.
(30) Larson, R. G. *J. Phys. II* **1996**, *6*, 1441.
(31) Yu, B.; Li, B. H.; Sun, P. C.; et al. *J. Chem. Phys.* **2005**, *123*.
(32) Gonzalez-Segredo, N.; Coveney, P. V. *Europhys. Lett.* **2004**, *65*, 795.
(33) Rychkov, I. *Macromol. Theory Simul.* **2005**, *14*, 207.
(34) Hamley, I. W.; Castelletto, V.; Mykhaylyk, O. O.; et al. *Langmuir* **2004**, *20*, 10785.
(35) Iacovella, C. R.; Keys, A. S.; Horsch, M. A.; et al. *Phys. Rev. E* **2007**, *75*, 040801.
(36) Chervanyov, A. I.; Balazs, A. C. *J. Chem. Phys.* **2003**, *119*, 3529.
(37) Huh, J.; Ginzburg, V. V.; Balazs, A. C. *Macromolecules* **2000**, *33*, 8085.
(38) Dotera, T.; Hatano, A. *J. Chem. Phys.* **1996**, *105*, 8413.
(39) Schultz, A. J.; Hall, C. K.; Genzer, J. *Macromolecules* **2005**, *38*, 3007.
(40) Frenkel D.; Smit, B. *Understanding Molecular Simulation*; Academic Press: San Diego, CA, 2002.
(41) Lyubartsev, A. P.; Martsinovski, A. A.; Shevkunov, S. V.; et al. *J. Chem. Phys.* **1992**, *96*, 1776.
(42) Wilding, N. B.; Muller, M. *J. Chem. Phys.* **1994**, *101*, 4324.
(43) Bennett, C. H. *J. Comput. Phys.* **1976**, *22*, 245.
(44) Trebst, S.; Huse, D. A.; Troyer, M. *Phys. Rev. E* **2004**, *70*.
(45) Cochran, E. W.; Bates, F. S. *Phys. Rev. Lett.* **2004**, *93*.

MA071449G